Simultaneous Observations of the June 23, 2015, Intense Storm at Low Earth Orbit and Geostationary Transfer Orbit

Viviane Pierrard, Alexandre Winant, Edith Botek, Jean-François Ripoll, Mélanie Cosmides, David M. Malaspina, Geoffrey D. Reeves, and Scott A. Thaller

Abstract – The electron fluxes in the outer radiation belt during and after the intense geomagnetic storm of June 23, 2015, are investigated both at polar low earth orbit (LEO) and geostationary transfer orbit (GTO). We use the Energetic Particle Telescope (EPT) instrument on board the European Space Agency PROBA-V satellite at LEO at 820 km of altitude and compare simultaneous observations of the Magnetic Electron Ion Spectrometer instrument on board the NASA Van Allen Probes circulating on a low inclination elliptical GTO orbit, ranging from 600 km to 30,600 km. In addition, we use the Electric Field and Waves instrument and the Electric and Magnetic Field Instrument Suite and Integrated Science to compile both the strength of the whistler waves associated to the storm dynamics and the cold electron density of the plasmasphere and plasma trough where the main wave–particle interactions (WPI) occur. From them, we extract mean wave properties to allow WPI and Fokker–Planck computations in a near future. We find that the equatorial trapped electron fluxes observed at GTO are generally higher than at LEO but with magnitudes depending on the energy. Below 1 MeV, maximal fluxes differ by about two orders of magnitude. However, the EPT ultrarelativistic flux (>2.4 MeV) is much lower than the Van Allen Probes flux at 2.33 MeV, by four to five orders of magnitude. During the storm, the dropout and flux increase observed at LEO and GTO present very similar shapes in L and energy versus time but with different intensities.

Manuscript received 26 September 2022.

Viviane Pierrard, Alexandre Winant, and Edith Botek are with the Department Space Physics and Solar-Terrestrial Center of Excellence, Royal Belgian Institute for Space Aeronomy, 3 av. Circulaire, Brussels, B-1180, Belgium; e-mail: viviane.pierrard@aeronomie.be, alexandre.winant@aeronomie.be, edith.botek@aeronomie.be.

Viviane Pierrard and Alexandre Winant are also with the Center for Space Radiations, ELI-C, Université Catholique de Louvain, Louvain-La-Neuve, Belgium.

Jean-François Ripoll and Mélanie Cosmides are with Commissariat à l'Energie Atomique, DAM, DIF, F-91297 Arpajon, France and with UPS, CEA, LMCE, 91680 Bruyères-le-Châtel, France; e-mail: Jean-Francois.Ripoll@cea.fr, melanie.cosmides@cea.fr.

David M. Malaspina is with the Astrophysical and Planetary Sciences Department, University of Colorado, Boulder, CO, 80309, USA and Laboratory for Atmospheric and Space Physics, University of Colorado, Boulder, CO 80309, USA; e-mail: David.Malaspina@colorado.edu.

Geoffrey D. Reeves is with the Los Alamos National Laboratory, Los Alamos, NM 87545, USA; e-mail: geoff@reevesresearch.org.

Scott A. Thaller is with the Laboratory for Atmospheric and Space Physics, University of Colorado, Boulder, CO 80309, USA; e-mail: Scott.Thaller@lasp.colorado.edu.

1. Introduction

The European Space Agency satellite PROBA-V provided flux observations from Energetic Particle Telescope (EPT) on a low earth orbit (LEO) polar orbit at an altitude of 820 km since its launch in May 2013. The inclination is 98.73°, the orbital rotation period has a duration of 101.21 min, and 10:30 A.M. is the nominal local time at the descending node. The EPT detector measures the electron fluxes above 500 keV, in addition to protons above 9.5 MeV [1].

The NASA Van Allen Probes mission, formerly called *Radiation Belt Storm Probes* (RPSP A and B) was launched in 2012 [2]. It operated simultaneously with EPT from 2013 to 2019, enabling unprecedented studies of the electron radiation belt variability in response to solar activity. RBSP flew on a low inclination (<20°) elliptical orbit ranging from 600 km to 30,600 km. The Magnetic Electron Ion Spectrometer (MagEIS) instrument observed electrons in the energy range from 30 keV to 4 MeV. MagEIS is made of four magnetic spectrometers aboard each of the two spacecraft, one low-energy unit (20 keV to 240 keV), two medium-energy units (80 keV to 1200 keV), and a high-energy unit (800 keV to 4800 keV), allowing us to analyze the spin-averaged radiation fluxes at lower energies than EPT and over thinner energy bands.

The plasma density is determined by the RBSP Magnetic Field Instrument Suite and Integrated Science (EMFISIS) instrument that measures the upper hybrid resonance frequency, completed by the spacecraft floating potential measured by the Electric Field and Waves (EFW) instrument when EMFISIS is unavailable. The comparison of electron fluxes measured by EPT at LEO with those of MagEIS close to the equatorial plane, combined with simulations, helps us understand the dynamics of the radiation belts [3].

2. Analysis of the Flux Observations

Figure 1 shows the EPT electron fluxes at LEO from June 18, 2015, up to June 28, 2015 (horizontal axis), as a function of the McIlwain parameter L (vertical axis) for four electron energy channels. A very

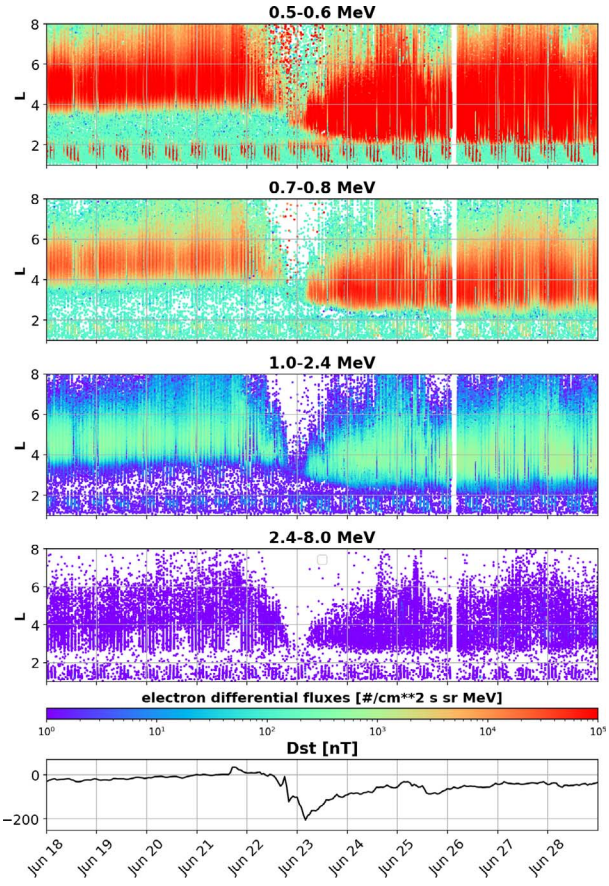

Figure 1. Electron fluxes observed by EPT at LEO from June 18 to 25, 2015, as a function of the McIlwain parameter L (vertical axis) and time (horizontal axis) for four electron energy channels. Bottom panel: Dst index.

intense storm was observed on June 23, 2015, with a disturbance storm time (Dst) index reaching –204 nT. Events of Dst below –125 nT represented 0.06% of events observed during the Van Allen Probes era. A massive dropout of the outer belt was clearly visible for all energy channels of EPT (>500 keV), as observed for all Dst events [3]. The dropout had a V-shape, i.e., started earlier, and had a longer duration at high L than at lower L. That V-shape well followed the Dst shape [4]. The dropout was followed by a strong flux enhancement in the outer belt and in the slot region to a lower L value compared with prestorm fluxes. We discuss in the following the occurrence of chorus waves and the wave power following the storm. Contrary to the dropout, electron penetration in the slot was only observed for the strongest storms, and the penetration depth was proportional to the Dst intensity [4]. It even reached the inner belt for the lower energies until the 1.2 MeV channel, but not for the next EPT channel at $E > 2.4$ MeV [5]. After the storm, the flux gradually decayed with time, especially in the slot region that reappeared a few days after the storms [6]. The correspondence of the slot region with the presence of whistler mode hiss waves in the equatorial plane is

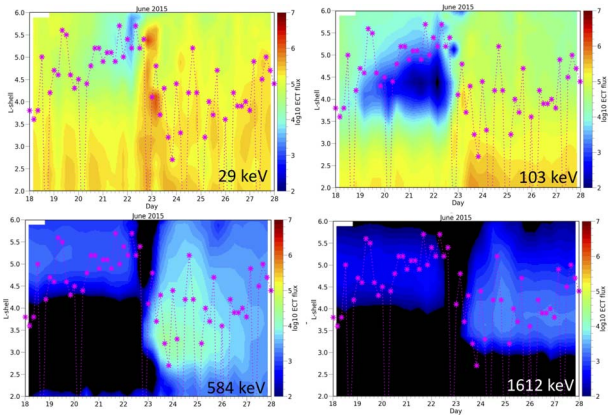

Figure 2. Electron fluxes (#/(cm^2 s sr keV)) versus time and L shell from June 18 to 25, 2015, as in Figure 1 but measured in the magnetic equatorial plane at GTO by RBSP-B. The first panel shows low-energy seed electrons (29 keV), contributing to the electromagnetic environment and as source of aurora. The three other panels show radiation belt ECT flux versus time and L shell for subrelativistic and relativistic electrons (0.103 MeV, 0.584 MeV, and 1.612 MeV). The magenta line corresponds to the plasmapause position extracted from spacecraft charging density (RBSP-B/EFW) following the method given in [8].

shown in the following (compare Figure 4 and related text). The enhancement of 1.2 MeV to 2.4 MeV electrons starting on June 24, 2015, was also associated with chorus activity. There was almost no electron flux with $E > 2.4$ MeV in the inner belt, probably due to low rate of radial diffusion at low L shell creating a barrier [7], limiting the penetration of these electrons at distances closer to the Earth [4].

Figure 2 shows RBSP-B observations using the Energetic Particle, Composition, and Thermal Plasma (ECT) combined flux [9] at geostationary transfer orbit (GTO) for the same period from June 18 to 28, 2015. At subrelativistic and relativistic energy above 0.5 MeV (last two panels), the radiation belt was concentrated in the outer belt above $L \sim 4$ before the storm of June 23, 2015, and a slot was clearly visible below, contrary to what was observed at lower energies (two first panels), where the more intense fluxes were concentrated at $L < 4$, with an outer edge increasing in L when E decreases. During the quiet period, relativistic electrons ($E > 1$ MeV) penetrated to lower L than subrelativistic electrons, because subrelativistic electrons ($\sim<1$ MeV) were more sensitive to whistler mode hiss waves scattering (see the following) than higher energy electrons, with these interactions occurring at higher L shell for the subrelativistic electrons and caused more scattering, especially during extended quiet periods [10–12].

In Figure 2, the dropout had also some trace of a V-shape, though not as clear as at LEO. The V-shape seemed to penetrate at lower L when the energy was high ($L \sim 4.5$ at 584 keV versus $L \sim 4$ at $L > 1$ MeV). This was also observed with EPT at LEO but with a lower penetration ($L \sim 3.9$ at 500 keV versus $L \sim 3$ at $E > 2.4$ MeV). At energies $E < 103$ keV, the dropout was

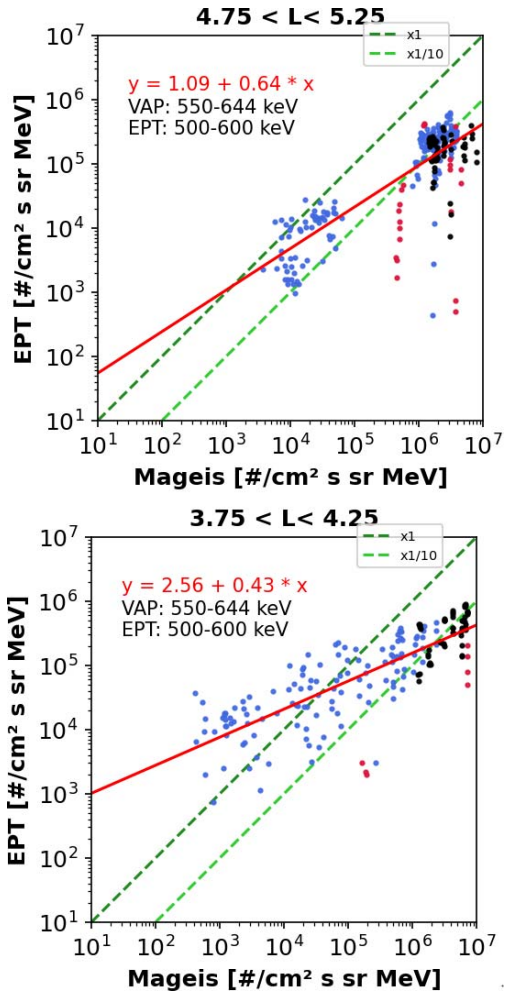

Figure 3. Scatterplots ($\log_{10}$ to $\log_{10}$) of 15 s-averaged differential fluxes from PROBA-V/EPT versus RBSP-A/MagEIS at 500keV to 600 keV when both spacecraft are at (top panel) $L = 5 \pm 0.25$ and (bottom panel) at $L = 4 \pm 0.25$. Blue dots: from June 1 to 22, 2015, before the storm; red dots: during the main phase of the storm, including dropouts; black dots: from June 24 to 30, 2015, after the storm.

hardly visible, which was an interesting feature, as dropout by definition should remove all particles at the same time, regardless the energy. This suggests fast refilling, for instance, from substorm injections occurring in a close time frame. The temporal binning of the flux generated in Figure 2 may also be too coarse to analyze the details of these fast processes. During the storm, the flux penetration at lower L was also clearly observed, with an injection reaching the inner belt up to $E = 584$ keV such as in EPT measurements; see [13]. We found dropout events were more intense at low altitude in the polar regions with EPT measurements than close to the equator with MagEIS.

3. Simultaneous EPT/MAGEIS Observations

To better understand the correspondence between LEO and GTO fluxes, we looked at the correspondence from a statistical point of view. Figure 3 presents scatterplots of the differential fluxes observed by EPT in the (500 keV to 600 keV) energy range plotted versus simultaneous MagEIS flux in the 550 keV to 644 keV energy range when the McIlwain parameter is $L = 5 \pm 0.25$ (top panel) and $L = 4 \pm 0.25$ (bottom panel) in June 2015. Data from June 1 to 22, 2015 (before the storm), are illustrated in blue. Each dot represents an averaged flux over 15 s. Low fluxes corresponded to beginning of June, while high fluxes were due to a first storm appearing on June 8, 2015. Observations during the main phase of the storm from June 22 to 23, 2015, are indicated with red dots for contrasting. Although a decrease of the flux was observed during the dropout by both instruments, fluxes observed by EPT at LEO were much lower than those observed at the equator by MagEIS (almost vertical dots). Fluxes observed by MagEIS during the storm but after the dropout were also further increased, while this was not seen in EPT measurements.

The similar vertically aligned blue dots were due to the dropout of the June 8, 2015, storm. The black dots correspond to the fluxes after the storm, which were already high due to the previous storm at this L range. In Figure 3, the parameters of the red regression line are based on all 307 fluxes measured in June 2015. The green lines show a slope of factor $\times 1$, indicative of exact correspondence, as well as $\times 10^{-1}$. We found an alignment between the EPT and MagEIS simultaneous flux observations at similar L, even if taken at different latitudes of the outer belt, with a good Pearson correlation coefficient (CC) = 0.78 at $L = 5$ and CC = 0.80 at $L = 4$, and a standard error (SE) = 0.035 and SE = 0.024, respectively. For small pitch-angle electrons observed by MagEIS, a better agreement between the observations was obtained, as shown in [14], where many other cases were presented; all show a clear correlation between EPT and MagEIS, with a slope always lower than 1. The flux was generally stronger at the equator, except at low L values close to the slot, and when the fluxes were low.

4. Whistler Wave Observations

Figure 4 shows the whistler hiss (50 Hz to 2000 Hz) and chorus ($>0.1\ f_{ce}$) identified following the method in [15, 16] from RBSP-B/EMFISIS in the equatorial region. Wave properties were extracted for EMFISIS at a 6 s rate and averaged before (June 18 to 21, 2015) and after (June 22 to 27, 2015) the storm for conditions, which are similar enough to justify taking the average. Clear differences between quiet and storm times were visible. Data were averaged on all Magnetic Local Time, but RBSP-B apogee was on the dusk side when measurements were done. The first quiet period was characterized by a dominance of hiss up to $L \sim 5$, with stable mean frequency ($\sim$350 Hz in Figure 4c) and small to moderate mean wave normal angle increasing abruptly from 20° to 40° at low $L \sim < 2.5$ (Figure 4d). There was a statistical overlap in the $L \sim 4$–5 (quiet)

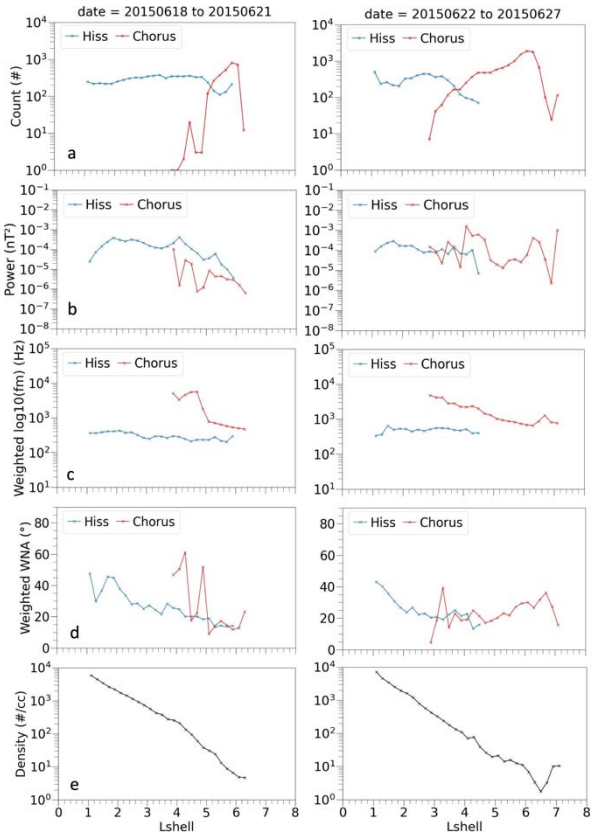

Figure 4. Whistler (blue) hiss and (red) chorus properties (left) before and (right) after the storm at GTO (from top to bottom: (a) number of 6 s measurements (counts); (b) mean power; (c) mean frequency; (d) mean wave normal angle; and (e) mean cold plasma electron density).

and $L \sim 3$–4 (storm) regions of hiss and chorus corresponding with the plasmapause region (L_{pp} located in the ∼100 #/cm^{-3} region of the plasma density in Figure 4e), where properties became more variable and oscillating but with low counts (Figure 4a). The active period had, in turn, significant hiss power confined in the dense plasmasphere below $L \sim 3$, adjacent intense chorus at $L \sim 4$, and a second peak power at $L \sim 6$ (Figure 4b). Chorus had this typical decreasing frequency following the cyclotron frequency (Figure 4c). The mean wave normal angle is also rather low (∼20°) and slightly increased for L increasing ($L > 4$), unless low counts ($L \sim L_{pp} \sim 3$–4; Figure 4d).

Connecting the occurrence of these waves back to the flux observations, hiss waves should cause loss before and during the storm up to $L = 5$ and explain the energy dependence of the loss in Figures 1 and 2. The pitch angle scattering they caused through diffusion occured in the loss cone region, at high latitude, where LEO satellites were. Thus, particle measurements from LEO satellites were key to relate the observed electron loss (or flux diminution) to the presence of waves and particles observed at higher latitudes by RBSP. Conversely, chorus should locally accelerate electrons in the $L \sim 4$ and $L \sim 6$ regions, as we saw occurring ∼1 day after the storm on June 24, 2015, until June 27, 2015, in the 1.2 MeV and 2.4 MeV EPT flux channel in Figure 1. The demonstration will come from future quasilinear simulations based on these new wave properties and the CEA CEVA radiation belt code [10, 11].

5. Discussion and Conclusions

The present analysis of the June 23, 2015, geomagnetic storm showed that dropouts were observed at all energies and orbits but were more visible for $E >$ 500 keV and at LEO. Dropouts seemed more intense at LEO or were at least more visible and for longer times. We suggest this is related to the occurrence of more injections in the equatorial plane from the magnetotail, which replenish faster dropouts in the equatorial region. This shows the importance of comparing simultaneous observations taken at different latitudes. LEO flux measurements are important to demonstrate the intensity of wave–particle interactions (WPI) occurring all along the field line, until eventually electrons precipitate in the field of view of LEO satellites. Other comparisons of magnetopause position and dropout depth indicated that dropouts were the consequence of magnetopause shadowing, i.e., the removal of the outer radiation belt electrons from the inner magnetosphere when a higher flux of solar wind pushes the magnetopause closer to the Earth [13]. Simulations of the particle motion also show that the dropout was also due to the outward drift motion of the particles associated to the perturbation of the magnetic field [13].

The gradual flux decay observed after the storm in the slot and the outer belt in the 0.1 MeV to 1 MeV range seems more related to WPI, especially with plasmaspheric hiss [10–12]. Due to the strong interactions between energetic particles trapped in the radiation belts and plasmaspheric hiss, the exact position of the plasmapause boundary, as well as the density of the low-energy background particles inside and outside the plasmasphere is critical to know [17]. The EMFISIS and EFW instruments on board Van Allen Probes allowed the deduction of the plasmapause position, as shown in Figure 2 (magenta dots) [8]. When no observations are available, the Space Weather Integrated Forecasting Framework plasmasphere model can be used to determine the position of the plasmapause and the density inside and outside the plasmasphere [18]. The model has been recently improved for the plasma trough part by using Van Allen Probes observations outside the plasmasphere [19].

With the observed wave conditions from June 18 to 27 2015, whistler hiss and chorus waves dominate WPI. More generally, other waves can also cause the loss of electrons, including those with anthropogenic origins: the very low frequency transmitter in the Northwest Cape of Australia has recently been observed to pitch-angle scatter electrons up to 800 keV, using EPT measurements [20]. The radiation belt particles also interact with the other regions of the magneto-

sphere, as attested by the observed links between the plasmapause, the ionospheric convection, the boundaries of the radiation belts, and the auroral oval [12].

6. Acknowledgments

The authors thank the CSR team for the Energetic Particle Telescope data validation and the Electric Field and Waves, Electric and Magnetic Field Instrument Suite and Integrated Science, and Magnetic Electron Ion Spectrometer teams of the Van Allen Probes mission for support. The authors thank the International Space Science Institute (ISSI) in Bern, through ISSI International Team project #477 (Radiation Belt Physics From Top To Bottom). The project 21GRD02 BIOSPHERE has received funding from the European Partnership on Metrology, co-financed by the European Union's Horizon Europe Research and Innovation Programme and by the Participating States. This work has received funding from the European Union's Horizon 2020 research and innovation programme under grant agreement No 101007599 for the PITHIA-NRF project.

7. References

1. V. Pierrard, G. Lopez Rosson, K. Borremans, J. Lemaire, J. Maes, et al., ¨The Energetic Particle Telescope: First Results," *Space Science Reviews*, **184**, 1, October 2014, pp. 87-106.
2. B. H. Mauk, N. J. Fox, S. G. Kanekal, D. G. Sibeck, and A. Ukhorskiy, "Science Objectives and Rationale for the Radiation Belt Storm Probes Mission," *Space Science Reviews*, **179** (1-4), 2013, pp. 3-27.
3. J.-F. Ripoll, S. G. Claudepierre, A. Y. Ukhorskiy, C. Colpitts, X. Li, et al., "Particle Dynamics in the Earth's Radiation Belts: Review of Current Research and Open Questions," *Journal of Geophysical Research: Space Physics*, **125**, 5, May 2020, p. e2019JA026735.
4. V. Pierrard, E. Botek, J.-F. Ripoll, and G. S. Cunningham, "Electron Dropout Events and Flux Enhancements Associated With Geomagnetic Storms Observed by PROBA-V/EPT From 2013 to 2019," *Journal of Geophysical Research: Space Physics*, **125**, 12, December 2020, p. e2020JA028487.
5. V. Pierrard, G. Lopez Rosson, and E. Botek, "Dynamics of Megaelectron Volt Electrons Observed in the Inner Belt by PROBA-V/EPT," *Journal of Geophysical Research: Space Physics*, **124**, 3, March 2019, pp. 1651-1659.
6. V. Pierrard and G. Lopez Rosson, "The Effects of the Big Storm Events in the First Half of 2015 on the Radiation Belts Observed by EPT/PROBA-V," *Annales Geophysicae*, **34**, 1, January 2016, pp. 75-84.
7. D. N. Baker, N. Jaynes, V. C. Hoxie, R. M. Thorne, J. C. Foster, et al., "An Impenetrable Barrier to Ultrarelativistic Electrons in the Van Allen Radiation Belts," *Nature*, **515**, November 2014, pp. 531–534.
8. J.-F. Ripoll, S. A. Thaller, D. P. Hartley, G. S. Cunningham, V. Pierrard, et al., "Statistics and Empirical Models of the Plasmasphere Boundaries From the Van Allen Probes for Radiation Belt Physics," *Geophysical Research Letters*, **49**, 21, November 2022, p. e2022GL101402.
9. A. J. Boyd, G. D. Reeves, H. E. Spence, H. O. Funsten, B. A. Larsen, et al., "RBSP-ECT Combined Spin-Averaged Electron Flux Data Product," *Journal of Geophysical Research: Space Physics*, **124**, 11, November 2019, pp. 9124–9136.
10. J.-F. Ripoll, G. D. Reeves, G. S. Cunningham, V. Loridan, M. Denton, et al., "Reproducing the Observed Energy-Dependent Structure of Earth's Electron Radiation Belts During Storm Recovery With an Event-Specific Diffusion Model," *Geophysical Research Letters*, **43**, 11, June 2016, pp. 5616–5625.
11. J.-F. Ripoll, V. Loridan, M. H. Denton, G. Cunningham, G. Reeves, et al., "Observations and Fokker-Planck Simulations of the *L*-Shell, Energy, and Pitch Angle Structure of Earth's Electron Radiation Belts During Quiet Times," *Journal of Geophysical Research: Space Physics*, **124**, 2, February 2019, pp. 1125–1142.
12. V. Pierrard, E Botek, J.-F. Ripoll, S. A. Thaller, M. B. Moldwin, et al., "Links of the Plasmapause With Other Boundary Layers of the Magnetosphere: Ionospheric Convection, Radiation Belts Boundaries, Auroral Oval," *Frontiers in Astronomy and Space Sciences*, **8**, November 2021, p. 728531.
13. V. Pierrard, J. F. Ripoll, G. Cunningham, E. Botek, O. Santolik, et al., "Observations and Simulations of Dropout Events and Flux Enhancements in October 2013: Comparing MEO Equatorial With LEO Polar Orbit," *Journal of Geophysical Research: Space Physics*, **126**, 6, May 2021, p. e2020JA028850.
14. A. Winant, "Study of the Terrestrial Radiation Belt (Using PROBA-V/EPT and RBSP/MagEIS)," Master thesis, Université catholique de Louvain, Louvain-La-Neuve, 2022.
15. D. M. Malaspina, A. N. Jaynes, C. Boule, J. Bortnik, S. A. Thaller, et al., "The Distribution of Plasmaspheric Hiss Wave Power With Respect to Plasmapause Location," *Geophysical Research Letters*, **43**, 15, August 2016, pp. 7878–7886.
16. D. M. Malaspina, A. N. Jaynes, S. Elkington, A. Chan, G. Hospodarsky, et al., "Testing the Organization of Lower-Band Whistler-Mode Chorus Wave Properties by Plasmapause Location," *Journal of Geophysical Research: Space Physics*, **126**, 1, January 2021, p. e2020JA028458.
17. N. Dahmen, A. Sicard, A. Brunet, O. Santolik, V. Pierrard, et al., "FARWEST: Efficient Computation of Wave-Particle Interactions for a Dynamic Description of the Electron Radiation Belt Diffusion," *Journal of Geophysical Research: Space Physics*, **127**, 10, September 2022, e2022JA030518.
18. V. Pierrard, E. Botek, and F. Darrouzet, "Improving Predictions of the 3D Dynamic Model of the Plasmasphere," *Frontiers in Astronomy and Space Science*, **8**, May 2021, p. 681401.
19. E. Botek, V. Pierrard, and F. Darrouzet, "Assessment of the Earth's Cold Plasmatrough Modeling by Using Van Allen Probes/EMFISIS and Arase/PWE Electron Density Data," *Journal of Geophysical Research: Space Physics*, **126**, 12, December 2021, p. E2021JA029737.
20. G. S. Cunningham, et al., "Observation of High-Energy Electrons Precipitated by NWC Transmitter From PROBA-V Low-Earth Orbit Satellite," *Geophysical Research Letters*, **47**, 16, July 2020, p. e2020GL089077.